



**CHALMERS**  
UNIVERSITY OF TECHNOLOGY

## **Experimental benchmarking of dielectric models for simulating the localized surface plasmon resonance in Au-Ag alloy nanospheres**

Downloaded from: <https://research.chalmers.se>, 2026-05-10 20:07 UTC


Citation for the original published paper (version of record):

Magyar, Z., Horváth, V., Jönsson, L. et al (2026). Experimental benchmarking of dielectric models for simulating the localized surface plasmon resonance in Au-Ag alloy nanospheres. *Materials Today Communications*, 51. <http://dx.doi.org/10.1016/j.mtcomm.2026.114920>

N.B. When citing this work, cite the original published paper.



## Experimental benchmarking of dielectric models for simulating the localized surface plasmon resonance in Au-Ag alloy nanospheres

Zsófia Magyar<sup>a,b</sup>, Viktória Horváth<sup>a</sup>, Linnéa Jönsson<sup>c</sup>, Zsuzsanna Pápa<sup>d</sup>, Maria E. Messing<sup>c,e</sup>, Attila Kohut<sup>a,\*</sup> 

<sup>a</sup> Department of Optics and Quantum Electronics, University of Szeged, Dóm sq. 9, Szeged 6720, Hungary

<sup>b</sup> SZTE Báthory István Practice Secondary School and Primary School, Szentháromság str. 2, Szeged 6722, Hungary

<sup>c</sup> Solid State Physics and NanoLund, Lund University, Professorsgatan 1B, Lund 221 00, Sweden

<sup>d</sup> ELI-ALPS Research Institute, ELI-HU Nonprofit Kft., Wolfgang Sandner str. 3, Szeged 6720, Hungary

<sup>e</sup> Quantum Device Physics Laboratory, Department of Microtechnology and Nanoscience, Chalmers University of Technology, Gothenburg 412 96, Sweden

### ARTICLE INFO

#### Keywords:

Localized surface plasmon resonance  
Dielectric function  
Gold-silver alloy nanoparticles  
Spark ablation

### ABSTRACT

The optical response of gold-silver (Au-Ag) alloy nanoparticles is strongly influenced by their localized surface plasmon resonance (LSPR), which can be tuned by varying the particle composition. Accurate simulation of LSPR, often performed using Mie theory, critically depends on the choice of dielectric function, yet available datasets for gold, silver, and their alloys vary widely. In this work, we aim to demonstrate how different dielectric functions lead to discrepancies in simulated LSPR wavelengths, even for pure metals. By using numerical simulation tools, such as PyMieLab and the miepython library, we systematically evaluate commonly used dielectric models for Au-Ag alloys by comparing their predicted LSPR wavelengths with experimental measurements obtained from spark-ablation-generated nanoparticles with well-defined compositions and narrow size distributions. The composition-dependent experimental LSPR data – obtained for the whole composition range between pure silver and gold – provides a reliable benchmark for assessing the accuracy of each model. Our results highlight the potential uncertainty introduced by different dielectric functions and help to identify a model which describes experimental data the best. The results underline the importance of dielectric model selection for predictive optical simulations of alloy nanoparticles.

### 1. Introduction

Gold and silver nanoparticles play a key role in plasmonic research due to their favorable optical properties, manifesting in strong localized surface plasmon resonance (LSPR) in the visible wavelength range [1,2]. Applications relying on the increased absorption and scattering near the resonance wavelength or the associated near-field enhancement utilize various approaches to engineer the desired particle properties [3–6]. One particularly potent way to tune the LSPR and hence the optical response of a nanomaterial is alloying various metals, such as gold and silver [7–11]. It is well known that by means of alloying gold and silver the LSPR of the material can be continuously shifted within a wide wavelength range set by the properties of the pure metals and hence the corresponding plasmonic effects can also be tuned on demand [7,12]. The synthesis of such materials is a routine task nowadays, either via chemical [13,14] or physical [15–18] methods. Characterization of the

LSPR of the produced nanoparticles is also routinely performed, mostly via measuring their extinction spectrum [12,19–21]. Such measurements are often used as a first, qualitative indicator of alloy formation or for composition estimation based on the position of the LSPR peak [22–24]. In principle, quantitative information on the alloy properties, such as composition, could also be deduced from the extinction spectra, however, this would require the precise theoretical description of the LSPR of the generated sample. This task is predominantly tackled by using the so-called Mie theory, which gives the solution of the Maxwell equations under certain conditions [25]. Due to the various numerical tools available, the Mie theory-based simulation of the optical response of nanoparticles is a relatively easy task, however the dielectric function – or dielectric permittivity – of the nanoparticle material – as well as that of the environment – is needed as an input [21,26]. This causes a certain level of ambiguity in the simulation results, since many – potentially different – experimental and theoretical datasets exist in the literature

\* Corresponding author.

E-mail address: [kohut.attila@szte.hu](mailto:kohut.attila@szte.hu) (A. Kohut).

<https://doi.org/10.1016/j.mtcomm.2026.114920>

Received 2 December 2025; Received in revised form 15 February 2026; Accepted 24 February 2026

Available online 25 February 2026

2352-4928/© 2026 The Authors. Published by Elsevier Ltd. This is an open access article under the CC BY-NC license (<http://creativecommons.org/licenses/by-nc/4.0/>).

even for pure gold and silver [27,28]. When alloys of these metals are synthesized, the situation gets even more complicated since precise dielectric data is needed preferably in the whole composition range to be able to perform reliable nanoplasmonic simulations involving such alloys. Even though gold-silver alloys can routinely be synthesized in many ways, the existence of some ambiguity in their optical response is well reflected by the fact that there are contradicting studies in the literature reporting a linear [12,29], second order [30], or third order [31,32] variation of the LSPR as a function of the composition of the Au-Ag nanoparticles. It should be noted that despite the many synthesis routes developed to obtain gold-silver alloy nanoparticles there is still some controversy in the literature regarding what elemental distribution of Au and Ag atoms can be expected in these particles on the nanoscale [33]. Different studies have shown different extent of segregation of gold and silver, based on the exact experimental conditions [34–36]. The presence of potential inhomogeneities in the atomic distribution of the synthesized particles could explain some of the ambiguities in the literature and also strongly supports the need for well-characterized alloy nanoparticles, when subtle changes in their optical response are studied. In the present work, we exemplify the potential uncertainty of LSPR simulation caused by different dielectric function datasets in the example of pure gold and silver nanospheres. Moreover, we systematically compare four dielectric models for Au-Ag alloys used in the literature in terms of the LSPR wavelengths of Au-Ag nanospheres calculated using these models. We compare the simulation results with experimental data obtained on homogeneously alloyed Au-Ag nanoparticles synthesized by spark ablation [37–40]. In order to provide the closest possible realization of the ideal conditions used in the simulations, highly spherical, monodisperse particles were generated in the gas phase with highly uniform composition without any stabilizing agent and deposited onto a glass surface. These samples – which were thoroughly characterized in our previous study [38] – allowed a direct comparison of the measured and the simulated LSPR wavelength and thus to decide which theoretical dielectric model gives the most reliable predictions, especially when size-dependent electron oscillation dampening effects are also considered.

## 2. Materials and methods

Simulation of the LSPR of pure gold and silver nanoparticles has been carried out by using the PyMieLab\_v1.0 software [41]. Dielectric data for gold and silver were selected from the built-in library of this software, the source of which is the refractiveindex.info database [27]. For the simulation of the LSPR of gold-silver alloys a purpose-made Python code has been used, which is based on the *miepython* library [42]. Alloyed gold-silver dielectric data were taken from the works of Rioux et al. [26] and Pena-Rodriguez et al. [43]. For deriving the dielectric function of gold-silver alloyed nanoparticles by means of the linear combination of the data corresponding to pure gold and silver (for the details please see the text later) the analytical dielectric model of Rioux et al. was used [26]. The analytical formula for predicting the LSPR of alloyed Au-Ag nanospheres derived by Verbruggen et al. [32] was also used. The above analytical formulas were implemented in our python simulation script to systematically compare the different models at the same conditions. Our python code incorporated the calculation of the complex dielectric function at a given size and composition for the specified wavelength range – which was 270–1000 nm for most of the study – and to perform the calculation of the extinction cross section base on the *miepython* library. The LSPR peak positions were obtained from each calculated spectrum by the same protocol for all the models.

To compare the simulation results to experimental data, gold-silver nanospheres have been synthesized by means of spark ablation. Spark ablation is an atmospheric-pressure gas-phase technique, relying on the periodic ablation of two electrodes in a controlled gaseous environment. Due to the all-physical, aerosol nature of the process, highly pure nanoparticles can be synthesized [37]. The experimental procedure and

all the relevant conditions are described in detail elsewhere [38], where the same samples have been synthesized as we used for the present study. For the sake of clarity, we highlight here that pure gold and silver, as well as gold-silver alloy nanospheres have been synthesized with average gold atomic fractions (GAF) of 0.25, 0.5, and 0.75 with deviations from the average values not larger than 0.03 on a single-particle level. The particles went through heat treatment in the aerosol phase, ensuring highly spherical morphology. Monodisperse size-fractions of the generated particle populations were selected by a so-called differential mobility analyzer (DMA) and then deposited onto glass slides by means of electrostatic precipitation. The particle diameter for all samples was set to 20 nm, except for pure silver, where the diameter was 15 nm. In the case of silver, the relatively low overall particle yield did not allow for an efficient size selection, however, the size distribution after heat treatment was reasonably monodisperse. Samples were prepared with 5% surface coverage to avoid plasmonic coupling between neighboring particles. The samples were not coated or otherwise post-processed after fabrication. A scanning electron microscope (SEM, Zeiss, GeminiSEM 500) has been used to visualize the morphology of the samples. Extinction spectra of the samples were acquired by using a spectrophotometer (Shimadzu UV-2101PC). Further details on the experimental setup and particle characterization are given in the [Supporting Information \(SI\)](#).

## 3. Results and discussion

Various dielectric datasets exist for pure gold and silver, many of them conveniently compiled in the form of wavelength-dependent complex refractive indices in the refractiveindex.info online database [27]. The data include measurement results on bulk samples [44–46], thin films [26,47,48], as well as the results of theoretical models [49]. If we compare some of these datasets for gold and silver, plotting the real and imaginary parts of the refractive index separately, it is evident that these data are far from being identical (cf. Fig. S5). The deviations vary with wavelength, but if we focus only on the region where LSPR occurs for gold and silver – around 530 nm and 400 nm in water, respectively – the relative standard deviation (RSD) of the data – defined as the standard deviation divided by the mean – is the largest for  $n_{Ag}$  and smallest for  $k_{Au}$ , with values of 73% and 8%, respectively. These differences evidently get reflected in the LSPR of gold and silver nanoparticles numerically simulated using the data shown in Fig. S5. Fig. 1 shows the LSPR simulation results for single gold and silver nanospheres, having a diameter of 20 nm, surrounded by water. The largest difference for gold is 10 nm, while for silver the largest difference is as large as 30 nm.

Even if we consider some of the highest cited sources of the literature, such as Johnson and Christy and McPeak *et al.*, the 9 nm LSPR difference obtained for gold is somewhat surprisingly large considering how widely used and broadly studied the gold nanoparticles are. The ambiguity of the data is further increasing with gold-silver alloy nanoparticles. Since gold and silver form a solid solution at every composition an assumption commonly found in the literature is that the dielectric function of the Au-Ag alloy can be simply given as the linear combination or the weighted average of that of pure Au and Ag:

$$\varepsilon_{AuAg} = x\varepsilon_{Au} + (1 - x)\varepsilon_{Ag} \quad (1)$$

where  $x$  is the atomic fraction of Au within the alloy and  $\varepsilon$  refers to the complex dielectric function. Even though this approach is often used [50–53], its adequacy in describing the optical properties of the Au-Ag alloy is highly questionable from a physical point of view and it has been argued many times [12,32], even in the NIR region far from the interband transitions [54]. The issues with the linear combination approach suggest that for the reliable description of the optical properties of Au-Ag alloys, direct measurements should be performed, preferably in a wide composition range. Such measurements are mostly performed utilizing ellipsometry on bulk or thin film samples [26,54] of

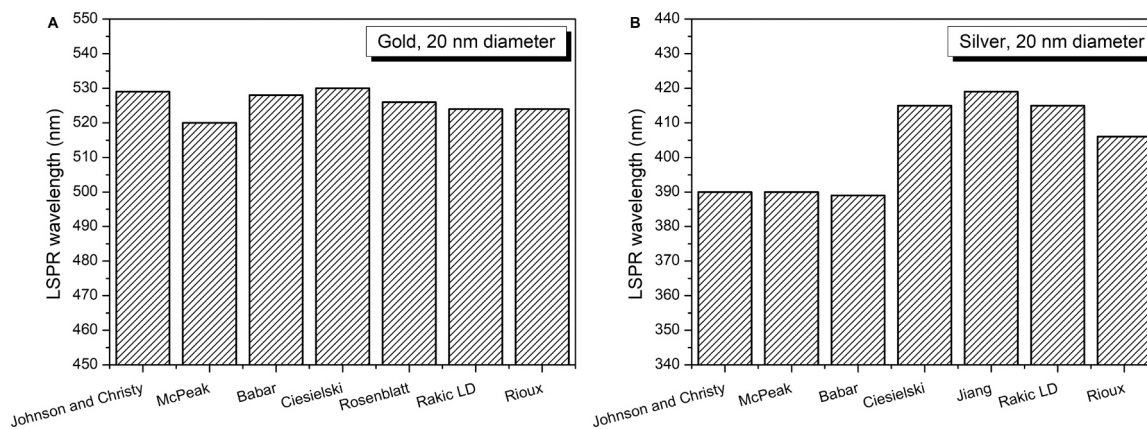


Fig. 1. LSPR wavelength of single gold (A) and silver (B) nanospheres with 20 nm diameter in water. Please note that the vertical axes do not start from zero.

a discrete set of compositions. The resulting tabulated databases are often not practical – in terms of their integrability to finite-difference time-domain (FDTD) simulations, for instance – so analytical models are more desirable. Even though the calculation of optical properties of plasmonic materials could be treated on a quantum level [55], the most prominent approach to obtain a continuous set of data for the Au-Ag alloy dielectric function is to use a Drude-Lorentz-type analytical formula and find the parameters fitting the experimental results the best [20,26,43,56]. In the following, the performance of such models will be evaluated.

To systematically assess the differences and similarities of various dielectric models describing Au-Ag alloys, the LSPR wavelength of single Au-Ag nanospheres were compared at different sizes and compositions. The extinction spectra of the nanoparticles were numerically simulated by using the analytical dielectric models taken from [26] and [43]. The weighted average dielectric function of Au-Ag – calculated by using Eq. 1 and the dielectric functions for pure Au and Ag from [26] – was also incorporated to the comparison for reference. Furthermore, the obtained LSPR data are compared to the predictions of the semiempirical model of Verbruggen *et al.* [32], which is based on a corrected version of the tabulated dielectric data from Ripken [57]. Therefore, LSPR prediction of four different approaches are compared to one another and to experimental data as well.

Simulation results are shown in Fig. 2A for single nanospheres of 50 nm diameter. Although it is often found to be a good approximation in Au-Ag alloy NP synthesis studies to assume a linear relationship between the gold content and the LSPR wavelength [12], it is clear from

Fig. 2 that none of the models' predictions are best described by a linear model. In fact, every model predicts slightly non-linear dependence of the LSPR wavelength on the composition. The analytical models of both Rioux *et al.* and Pena-Rodriguez *et al.* resulted in similar curves, with a shift of ca. 3–8 nm over the whole GAF range. The semiempirical model of Verbruggen *et al.* is reasonably close to that of Rioux *et al.* and Pena-Rodriguez *et al.* in the 0.1–0.6 GAF region but considerably deviates near pure silver – ca. 14 nm – and in the 0.6–0.9 GAF range – ca. 10 nm. As expected, the simple linear combination – or weighted average – model described by Eq. 1 deviates considerably from the other models, exhibiting a ca. 30 nm difference around 0.7 GAF. As a result of the comparison shown in Fig. 2A, there are distinct differences between the models discussed here. However, it is not clear which will describe the actual optical properties of Au-Ag alloy NPs best. To experimentally verify the predictions made by different dielectric models, Au-Ag alloy NPs were synthesized and analyzed in terms of their LSPR. For a meaningful comparison of simulation and measurement data it is crucial to ensure that the produced particles are highly monodisperse, have a very good compositional uniformity, and as close to perfect spheres as possible. Such particles can be synthesized in the gas phase via a technique called spark ablation [37]. Here we employed electrodes with predefined compositions – pure Ag, pure Au and 25 at% Au, 50 at% Au and 75 at% Au – in a controlled gaseous environment and used repetitive spark plasmas to release the atoms of the electrodes into the gas phase. For further details on the synthesis process please see the SI. As it was recently shown, the electrode composition is very closely preserved by the generated bimetallic particles, hence the compositional

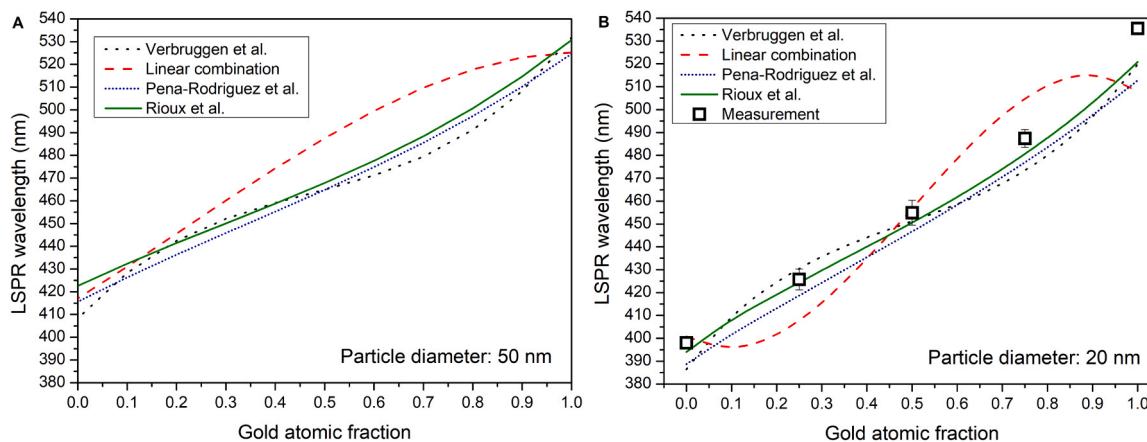


Fig. 2. Dependence of LSPR of 50 nm diameter Au-Ag nanospheres in water on the gold fraction simulated by using different dielectric models (A). Measured LSPR wavelength of 20 nm diameter Au-Ag NPs deposited onto glass substrates together with the corresponding simulation results based on different dielectric models. An effective dielectric constant of 1.63 is used for the surrounding medium (B).

uniformity is ensured [38]. Details on composition measurements can be found in the SI. It is important to note that in addition to composition, i. e., the Au-to-Ag ratio within the nanoparticles, their elemental distribution is important too. Since dielectric models assume homogeneous alloys, the synthesized particles need to meet this assumption too. As shown in Fig. S2 and the corresponding details in the SI, it can be reasonably stated that the nanoparticles investigated in the present study are indeed homogeneous alloys of Au and Ag.

To obtain a spherical shape, the produced aerosol particles are guided through a tube furnace for achieving perfect sintering. Then 20 nm diameter particles – 15 nm in case of silver – were selected still in the gas phase by using a static electric field. The resulting highly monodisperse, ultrapure Au-Ag nanospheres shown in Fig. 3 were deposited onto glass substrates for extinction measurements. A further important aspect to address from the perspective of comparing idealized simulations with experiments is the surface chemistry of the nanoparticle samples. By employing X-ray photoelectron spectroscopy (XPS) on each sample corresponding to different compositions we concluded that surface oxidation is not significant by the time of extinction measurements and its potential influence on the optical response is negligible. For details on the XPS analysis please see Table S1 and the related discussion in the SI.

The measurement results are shown together with the corresponding simulations in Fig. 2B. It should be noted that the extinction measurements of the prepared NPs were conducted in ambient air, while the particles were supported by glass microscope slides. In such cases the (effective) dielectric constant describing the surrounding medium of the metal NPs will be between the dielectric constants of air and glass, with an exact value depending on the contact surface of the particles and the substrate [58]. As a reasonable approximation, the average of the dielectric constants of air and glass can be used [59], which is 1.63 in the present case. We have shown by using an FDTD model of the experimental procedure – without assuming an effective dielectric constant – that this approach causes negligible error in predicting the LSPR wavelength of our system (for further details please see the SI). It is evident from Fig. 2B that none of the models describe perfectly the measured LSPR values, although the model of Rioux *et al.* exhibits a very good agreement, especially in the lower GAF range – below 0.5. The second-best fit is that of the model of Pena-Rodriguez *et al.*, followed by the semi-empirical model of Verbruggen *et al.*, followed by the simple linear combination model with the largest overall deviations. The quantitative data on the differences between the measured and simulated LSPR wavelengths are summarized in Fig. 4B.

Even though the model of Rioux *et al.* already provides a reasonably good agreement with the measurements – correctly predicting the overall non-linear composition-dependence and very closely

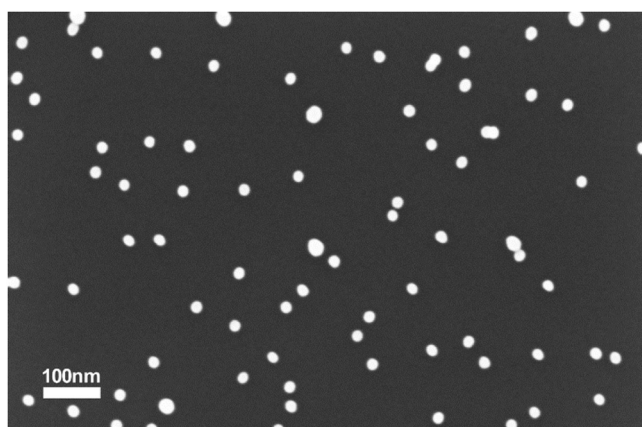


Fig. 3. SEM micrograph of 20 nm, 50 at% Au-Ag nanospheres deposited onto a Si substrate.

approximating the absolute LSPR values, there is an important factor, which was not considered yet. This is the so-called intrinsic size-dependence of the LSPR wavelength, which describes a particle size range, where the Mie theory does not predict size dependence. Although the so-called quasistatic approximation is fulfilled, the dielectric function of the metal nanoparticles starts to vary with size. This effect starts to emerge when the mean free path of the electrons becomes comparable to that of the particle size and hence surface effects also contribute to the dampening of the resonance [59], resulting in a shift of the LSPR band. For particle diameters below ca. 20 nm a red shift was experimentally found, also depending on the particle composition [60,61]. For very small silver clusters – below 1 nm – generally a blue shift is expected [55], while in an intermediate size range – ca. 1–10 nm – both blue- and red shifts were demonstrated depending on the materials system [62]. It has been shown that such apparent contradictions can be resolved by a mixed classical/quantum model, considering the local environment of the metal particles too [63]. A very simple approach for adjusting the dielectric function for – moderate, i. e. non-quantum – size effects is to include an extra dampening factor for the Drude contribution:

$$\Delta\Gamma(r) = A \frac{v_F}{r} \quad (2)$$

where  $A$  is a theory-dependent constant,  $r$  is the particle radius and  $v_F$  is the electrons' Fermi velocity, considered to be around  $1.4 \times 10^6 \text{ m s}^{-1}$  for gold, silver and their alloys. Rioux *et al.* proposed to include the correction factor described by Eq. 2 in their analytical model, with using  $A = 1$  [26]. The corresponding simulation results are shown in Fig. 4A, together with the measured data and the not size-corrected simulations. It is evident that the already reasonably good agreement became even better, which is especially remarkable considering that the simulation does not include any parameter fitting. The quantitative deviations between the predictions made by using the different models – including the size-corrected and not size-corrected models of Rioux *et al.* – and the measured data are shown in Fig. 4B. The smallest overall deviation is achieved in case of the size-corrected Rioux model, which is less than 2.5 nm for all the compositions except for the pure gold case, which is ca. 7.5 nm.

In addition to comparing the simulated data with the mean values of the measurements, we also evaluated the overall goodness of fit for different model predictions by considering the experimental uncertainty. To this end, the chi-square value was calculated for each case both for the whole GAF range investigated and also for a limited range, which does not include pure gold. The results are in line with the conclusions made based on Fig. 4B, that is the size-corrected Rioux model fits best, with the smallest overall chi-square value. Nevertheless, the analysis suggests that the prediction for pure gold deviates more from the experimental value than that could be explained by simple experimental uncertainty, suggesting additional factors that are not considered. Such factor can be the limitations of the simple size-correction term described by Eq. (2). However, if the point corresponding to pure gold is excluded, the chi-square values indicate that the calculated LSPR wavelengths are in line with the measurements for the size-corrected Rioux models and deviate considerably for the rest. More on the chi-square analysis can be found in the SI.

The above results show that different dielectric models of Au-Ag alloys found in the literature lead to different LSPR simulation results, the significance of which highly depending on the exact composition. It has been also shown that due to their good uniformity – both in terms of shape, size, and composition – the measured absorbance of spark ablation-generated Au-Ag NPs can serve as a reliable benchmark for assessing the validity of simulated data. As a result, it was found that the size-corrected analytical model of Rioux *et al.* is able to predict measurement data exceptionally well, provided that the particle samples are highly monodisperse, spherical and non-interacting.

As was shown above, the simple size-dependent correction term in the dielectric function (c.f. Eq. (2)) causes a noticeable red-shift in the

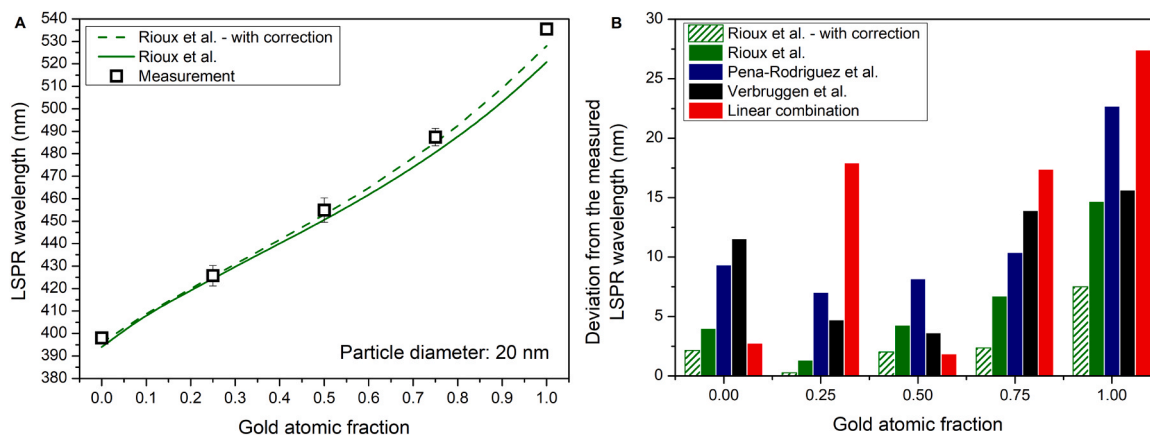


**Fig. 4.** Measured LSPR data together with simulation results based on the size-corrected and not size-corrected models of Rioux *et al.* for Au-Ag alloy NPs as a function of particle composition (A). Deviations from the measured LSPR wavelengths at different compositions for all the theoretical models studied here (B).

simulated LSPR wavelength, which is in line with the measurement results (c.f. Fig. 4). In order to visualize this size-related effect on a broader size and composition range, we numerically simulated the LSPR of Au-Ag nanospheres in the 0–1 GAF and 10–100 nm diameter range. The obtained three-dimensional surface is shown in Fig. 5.

The surface shown in Fig. 5 generalizes the results suggested by Fig. 4A that the size-correction described by Eq. (2) basically does not affect the case of pure silver particles and has an increasingly larger effect on the predicted LSPR wavelength with increasing gold content at small sizes (please see the red-shift of the LSPR wavelength for high GAF and sub-20 nm size). The experimental and simulation data shown above suggests that the choice of the dielectric function will affect the simulated LSPR wavelengths of Au-Ag alloy nanoparticles, especially at or below 20 nm. However, these effects might get “blurred” by potential experimental uncertainties in particle shape, size, or – most dominantly – composition. This is a potential reason for the apparent contradictions in experimental literature data on the exact function of the LSPR wavelength dependence on gold content. Nevertheless, the prediction of

the LSPR wavelength of Au-Ag alloy nanospheres is shown in Fig. 5, which is in good agreement with experimental data provided that the synthesized particles are sufficiently spherical, non-interacting, and monodisperse both in terms of size and composition. Although these conditions are not necessarily met in every experimental setting, we compared the experimental data taken from the highly cited paper of Link *et al.* [12] with simulated data from Fig. 5 at sizes and GAF corresponding to that of the experiments. The results are shown in Fig. 6, indicating a very good agreement for alloyed particles with a GAF of larger than 0.5, with slight deviations from the measured values only at the two ends of the composition range (i.e., at pure gold and close to pure silver). This comparison further strengthens the above results, showing that the size-corrected analytical dielectric model of Rioux *et al.* is able to accurately describe the LSPR wavelength of alloyed Au-Ag nanospheres, especially in the size range around 20 nm.

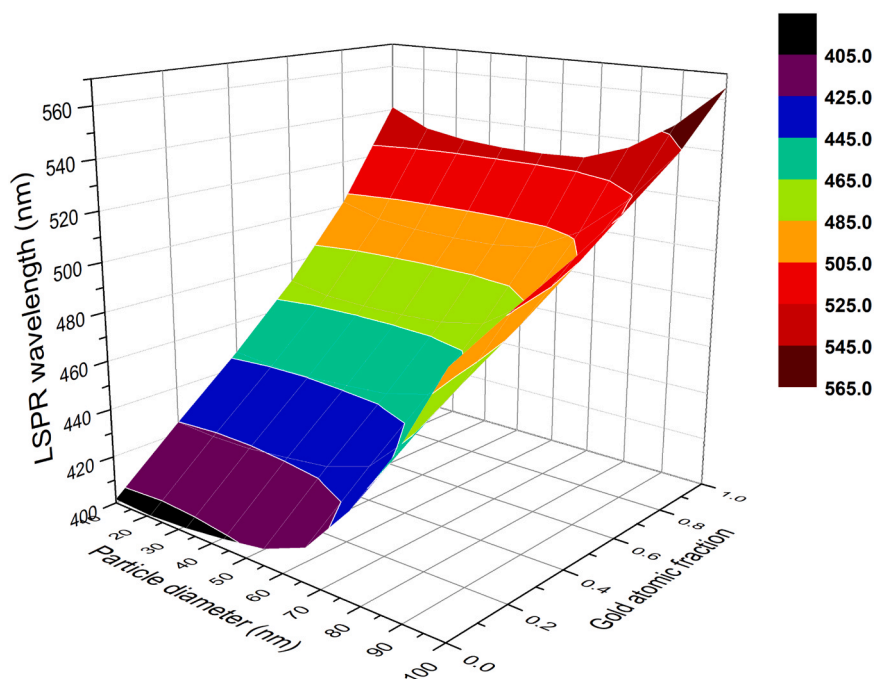


**Fig. 5.** LSPR wavelength simulated at a broad particle composition and size range by using the size-corrected dielectric function model by Rioux *et al.* The surrounding medium used in this simulation is water.

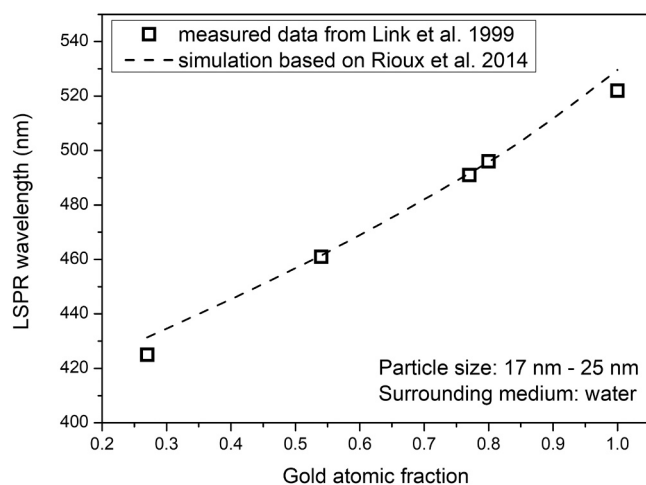


Fig. 6. Experimental LSPR data taken from Link *et al.*[12] together with the theoretical curve based on Fig. 5.

#### 4. Conclusions

In this study, we investigated the influence of the choice of dielectric function on the simulation of localized surface plasmon resonance (LSPR) in pure gold, silver and alloyed gold-silver nanospheres. Our results demonstrate that even for pure gold and silver nanoparticles, widely used dielectric datasets lead to significant variations – up to 30 nm in the LSPR peak wavelength – emphasizing the role of dielectric function selection in nanoplasmonic simulations. For Au-Ag alloy nanoparticles, we compared four different dielectric function models: a simple linear combination – also called as the weighted average – of the dielectric functions of pure Au and Ag, two analytical models, and a semi-empirical model. All models predicted nonlinear LSPR-composition dependence, in contrast to the often-assumed linear relationship and showed deviations from one another. We compared the simulation results with measured LSPR data of 20 nm Au-Ag alloyed nanospheres. By employing highly controlled experimental conditions – ultrapure, monodisperse, spherical Au-Ag nanospheres with well-defined compositions synthesized in the gas phase via spark ablation – we ensured that the experimental LSPR data could serve as a reliable benchmark. The simple linear combination model exhibited the poorest agreement with experimental results, with deviations up to ca. 25 nm. The analytical models of Rioux *et al.* and Pena-Rodríguez *et al.* showed significantly better performance, with Rioux *et al.*'s model providing the best agreement, especially after incorporating a correction factor for the so-called intrinsic size-dependence of the dielectric function. The overall difference between the measured and simulated LSPR peak wavelength for all the compositions investigated varied in the range of 2.5 nm to 7.5 nm with this model. Our findings highlight the important role of dielectric function choice in the simulation of the optical response of alloyed gold-silver nanostructures.

#### CRedit authorship contribution statement

**Attila Kohut:** Writing – review & editing, Writing – original draft, Supervision, Funding acquisition, Conceptualization. **Zsófia Magyar:** Writing – original draft, Investigation, Formal analysis, Data curation. **Zsuzsanna Pápa:** Writing – review & editing, Validation, Data curation. **Maria E. Messing:** Writing – review & editing, Supervision, Funding acquisition. **Viktória Horváth:** Validation, Software, Investigation. **Linnéa Jönsson:** Visualization, Methodology, Investigation, Data curation.

#### Declaration of Competing Interest

The authors declare that they have no known competing financial interests or personal relationships that could have appeared to influence the work reported in this paper.

#### Acknowledgments

We are grateful for the funding provided from the National Research, Development and Innovation Fund under the TKP2021-NVA-19, and 2022–2.1.1-NL-2022–00012 projects. This work was also supported by the Swedish Foundation for Strategic Research (Grant No. FFL18–0282) and by the Swedish Research Council (Grant No. 2023–05120). Z. Pápa and A. Kohut received a Bolyai Research Scholarship of the Hungarian Academy of Sciences (BO/00773/24 and BO/00444/25, respectively). The support from the University of Szeged Open Access Fund (Grant ID: 8277) is also greatly appreciated.

#### Appendix A. Supporting information

Supplementary data associated with this article can be found in the online version at doi:10.1016/j.mtcomm.2026.114920.

#### Data availability

Data will be made available on request.

#### References

- [1] K. Khurana, N. Jaggi, Localized surface plasmonic properties of Au and Ag nanoparticles for sensors: a review, *Plasmonics* 16 (2021) 981–999, <https://doi.org/10.1007/S11468-021-01381-1>.
- [2] K.M. Mayer, J.H. Hafner, Localized surface plasmon resonance sensors, *Chem. Rev.* 111 (2011) 3828–3857, <https://doi.org/10.1021/CR100313V/ASSET/CR100313V.FP.PNG.V03>.
- [3] Y. Sun, Y. Xia, Shape-controlled synthesis of gold and silver nanoparticles, *Science* 298 (1979) (2002) 2176–2179, <https://doi.org/10.1126/science.1077229>.
- [4] J.E. Millstone, S.J. Hurst, G.S. Métraux, J.I. Cutler, C.A. Mirkin, Colloidal gold and silver triangular nanoprisms, *Small* 5 (2009) 646–664, <https://doi.org/10.1002/SMLL.200801480>.
- [5] M. Mayer, A.M. Steiner, F. Röder, P. Formanek, T.A.F. König, A. Fery, Aqueous gold overgrowth of silver nanoparticles: merging the plasmonic properties of silver with the functionality of gold, *Angew. Chem. Int. Ed.* 56 (2017) 15866–15870, <https://doi.org/10.1002/ANIE.201708398>.
- [6] L. Lu, G. Burkey, I. Halaciuga, D.V. Goia, Core-shell gold/silver nanoparticles: synthesis and optical properties, *J. Colloid Interface Sci.* 392 (2013) 90–95, <https://doi.org/10.1016/J.JCIS.2012.09.057>.
- [7] M.Rebello Sousa Dias, M.S. Leite, Alloying: a platform for metallic materials with on-demand optical response, *Acc. Chem. Res.* 52 (2019) 2881–2891, [https://doi.org/10.1021/ACS.CCACCOUNTS.9B00153/ASSET/IMAGES/MEDIUM/AR-2019-00153T\\_0010.GIF](https://doi.org/10.1021/ACS.CCACCOUNTS.9B00153/ASSET/IMAGES/MEDIUM/AR-2019-00153T_0010.GIF).
- [8] G. Guisbiers, R. Mendoza-Cruz, L. Bazán-Díaz, J.J. Velázquez-Salazar, R. Mendoza-Perez, J.A. Robledo-Torres, J.L. Rodríguez-Lopez, J.M. Montejano-Carrizales, R. L. Whetten, M. José-Yacamán, Electrum, the gold-silver alloy, from the bulk scale to the nanoscale: synthesis, properties, and segregation rules, *ACS Nano* 10 (2016), <https://doi.org/10.1021/acsnano.5b05755>.
- [9] J. Feng, D. Chen, P.V. Pikhitsa, Y. ho Jung, J. Yang, M. Choi, Unconventional alloys confined in nanoparticles: building blocks for new matter, *Matter* 3 (2020) 1646–1663, <https://doi.org/10.1016/j.matt.2020.07.027>.
- [10] K.D. Gilroy, A. Ruditskiy, H.C. Peng, D. Qin, Y. Xia, Bimetallic nanocrystals: syntheses, properties, and applications, *Chem. Rev.* 116 (2016) 10414–10472, <https://doi.org/10.1021/acs.chemrev.6b00211>.
- [11] A. Kohut, A. Kéri, V. Horváth, J. Kopniczky, T. Ajtai, B. Hopp, G. Galbács, Z. Geretovszky, Facile and versatile substrate fabrication for surface enhanced Raman spectroscopy using spark discharge generation of Au/Ag nanoparticles, *Appl. Surf. Sci.* 531 (2020), <https://doi.org/10.1016/j.apsusc.2020.147268>.
- [12] S. Link, Z.L. Wang, M.A. El-Sayed, Alloy formation of gold-silver nanoparticles and the dependence of the plasmon absorption on their composition, *J. Phys. Chem. B* 103 (1999) 3529–3533, <https://doi.org/10.1021/JP990387W/ASSET/IMAGES/LARGE/JP990387WF00004.JPEG>.
- [13] D. Rioux, M. Meunier, Seeded growth synthesis of composition and size-controlled gold-silver alloy nanoparticles, *J. Phys. Chem. C* 119 (2015) 13160–13168, <https://doi.org/10.1021/acs.jpcc.5b02728>.
- [14] X. Situ, S.S. Bayram, A.S. Blum, Two-step synthesis of large gold-silver alloy nanoparticles via the combination of seeded growth and citrate co-reduction, *J. Phys. Chem. C* 127 (2023) 10888–10895, [https://doi.org/10.1021/ACS.JPC.3C03095/ASSET/IMAGES/LARGE/JP3C03095\\_0005.JPEG](https://doi.org/10.1021/ACS.JPC.3C03095/ASSET/IMAGES/LARGE/JP3C03095_0005.JPEG).

- [15] A. Kohut, L.P. Villy, A. Kéri, Á. Békéti, D. Megyeri, B. Hopp, G. Galbács, Z. Geretovszky, Full range tuning of the composition of Au/Ag binary nanoparticles by spark discharge generation, *Sci. Rep.* 11 (2021) 5117, <https://doi.org/10.1038/s41598-021-84392-6>.
- [16] Z. Homik, J. Kopiczky, T. Smausz, D. Berkesi, B. Hopp, Formation of gold/silver composite nanoparticles by pulsed laser ablation of gold–silver layered films in liquid, *Appl. Phys. A Mater. Sci. Process.* 128 (2022) 1–13, <https://doi.org/10.1007/S00339-022-05938-7/METRICS>.
- [17] I. Lee, S.W. Han, K. Kim, Production of Au–Ag alloy nanoparticles by laser ablation of bulk alloys, *Chem. Commun.* 3 (2001) 1782–1783, <https://doi.org/10.1039/b105437f>.
- [18] A. Kohut, L.P. Villy, L. Jönsson, D. Megyeri, G. Galbács, M.E. Messing, Z. Geretovszky, Gold–silver alloy nanoparticle formation via spark ablation: the dynamics of material mixing, *Nanoscale Adv.* (2025), <https://doi.org/10.1039/D4NA01076K>.
- [19] V. Amendola, M. Meneghetti, Size evaluation of gold nanoparticles by UV–vis spectroscopy, *J. Phys. Chem. C* 113 (2009) 4277–4285, [https://doi.org/10.1021/JP8082425/SUPPL\\_FILE/JP8082425\\_SI\\_001.PDF](https://doi.org/10.1021/JP8082425/SUPPL_FILE/JP8082425_SI_001.PDF).
- [20] M. Moskovits, I. Srnová-loufová, B. Vlková, Bimetallic Ag–Au nanoparticles: extracting meaningful optical constants from the surface-plasmon extinction spectrum, *J. Chem. Phys.* 116 (2002) 10435–10446, <https://doi.org/10.1063/1.1449943>.
- [21] A. Djorović, S.J. Oldenburg, J. Grand, E.C. Le Ru, Extinction-to-absorption ratio for sensitive determination of the size and dielectric function of gold nanoparticles, *ACS Nano* 14 (2020) 17597–17605, [https://doi.org/10.1021/ACS.NANO.0C08431/SUPPL\\_FILE/NNOC08431\\_SI\\_001.PDF](https://doi.org/10.1021/ACS.NANO.0C08431/SUPPL_FILE/NNOC08431_SI_001.PDF).
- [22] A. Pal, S. Shah, S. Devi, Synthesis of Au, Ag and Au–Ag alloy nanoparticles in aqueous polymer solution, *Colloids Surf. A Physicochem. Eng. Asp.* 302 (2007) 51–57, <https://doi.org/10.1016/j.colsurfa.2007.01.054>.
- [23] A.K. Samal, L. Polavarapu, S. Rodal-Cedeira, L.M. Liz-Marzán, J. Pérez-Juste, I. Pastoriza-Santos, Size tunable Au@Ag core-shell nanoparticles: synthesis and surface-enhanced raman scattering properties, *Langmuir* 29 (2013) 15076–15082, <https://doi.org/10.1021/la403707j>.
- [24] R.D. Averitt, S.L. Westcott, N.J. Halas, Linear optical properties of gold nanoshells, 1999.
- [25] J. Zhao, A.O. Pinchuk, J.M. McMahan, S. Li, L.K. Ausman, A.L. Atkinson, G. C. Schatz, Methods for describing the electromagnetic properties of silver and gold nanoparticles, *Acc. Chem. Res.* 41 (2008) 1710–1720, [https://doi.org/10.1021/AR800028J/ASSET/IMAGES/LARGE/AR-2008-00028J\\_0007.JPEG](https://doi.org/10.1021/AR800028J/ASSET/IMAGES/LARGE/AR-2008-00028J_0007.JPEG).
- [26] D. Rioux, S. Vallières, S. Besner, P. Muñoz, E. Mazur, M. Meunier, An analytic model for the dielectric function of Au, Ag, and their Alloys, *Adv. Opt. Mater.* 2 (2014) 176–182, <https://doi.org/10.1002/adom.201300457>.
- [27] M.N. Polyanskiy, Refractiveindex.info database of optical constants, *Sci. Data* 11 (2024) 1–19, <https://doi.org/10.1038/s41597-023-02898-2>.
- [28] R. Borah, S.W. Verbruggen, Silver-gold bimetallic alloy versus core-shell nanoparticles: implications for plasmonic enhancement and photothermal applications, *J. Phys. Chem. C* 124 (2020) 12081–12094, [https://doi.org/10.1021/ACS.JPC.0C02630/ASSET/IMAGES/LARGE/JPC02630\\_0009.JPEG](https://doi.org/10.1021/ACS.JPC.0C02630/ASSET/IMAGES/LARGE/JPC02630_0009.JPEG).
- [29] M.P. Mallin, C.J. Murphy, Solution-phase synthesis of sub-10 nm Au–Ag alloy nanoparticles, *Nano Lett.* 2 (2002) 1235–1237, <https://doi.org/10.1021/NL025774N/ASSET/IMAGES/LARGE/NL025774NF000003.JPEG>.
- [30] J. Zhu, Theoretical study of the optical absorption properties of Au–Ag bimetallic nanospheres, *Phys. E Low. Dimens. Syst. Nanostruct.* 27 (2005) 296–301, <https://doi.org/10.1016/j.physe.2004.12.006>.
- [31] V. Coviello, D. Forrer, V. Amendola, Recent developments in plasmonic alloy nanoparticles: synthesis, modelling, properties and applications, *ChemPhysChem* 23 (2022) e202200136, <https://doi.org/10.1002/CPHC.202200136>.
- [32] S.W. Verbruggen, M. Keulemans, J.A. Martens, S. Lenaerts, Predicting the surface plasmon resonance wavelength of gold–silver alloy nanoparticles, *J. Phys. Chem. C* 117 (2013) 19142–19145, <https://doi.org/10.1021/jp4070856>.
- [33] M. Moreira, E. Cottancin, M. Pellarin, L. Roiban, K. Masenelli-Varlot, D. Ugarte, V. Rodrigues, M. Hillenkamp, Intrinsic coexistence of miscibility and segregation in gold–silver nanoalloys, *Small* 21 (2025) 2411151, <https://doi.org/10.1002/SMLL.202411151>.
- [34] Q. Gromoff, P. Benzo, W.A. Saidi, C.M. Andolina, M.J. Casanove, T. Hungria, S. Barre, M. Benoit, J. Lam, Exploring the formation of gold/silver nanoalloys with gas-phase synthesis and machine-learning assisted simulations, *Nanoscale* 16 (2023) 384–393, <https://doi.org/10.1039/D3NR04471H>.
- [35] M. Lasserus, M. Schnedlitz, D. Knez, R. Messner, A. Schiffmann, F. Lackner, A. W. Hauser, F. Hofer, W.E. Ernst, Thermally induced alloying processes in a bimetallic system at the nanoscale: AgAu sub-5 nm core–shell particles studied at atomic resolution, *Nanoscale* 10 (2018) 2017–2024, <https://doi.org/10.1039/C7NR07286D>.
- [36] T.W. Liao, A. Yadav, K.J. Hu, J. Van Der Tol, S. Cosentino, F. D’Acapito, R. E. Palmer, C. Lenardi, R. Ferrando, D. Grandjean, P. Lievens, Unravelling the nucleation mechanism of bimetallic nanoparticles with composition-tunable core–shell arrangement, *Nanoscale* 10 (2018) 6684–6694, <https://doi.org/10.1039/C8NR01481G>.
- [37] A. Schmidt-Ott (Ed.), *Spark Ablation: Building Blocks for Nanotechnology*, Jenny Stanford Publishing, 2020.
- [38] L. Jönsson, M. Snellman, A.C. Eriksson, M. Kåredal, R. Wallenberg, S. Blomberg, A. Kohut, L. Hartman, M.E. Messing, The effect of electrode composition on bimetallic AgAu nanoparticles produced by spark ablation, *J. Aerosol Sci.* 177 (2024) 106333, <https://doi.org/10.1016/J.JAEROSCI.2023.106333>.
- [39] A. Kohut, L.P. Villy, T. Ajtai, Z. Geretovszky, G. Galbács, The effect of circuit resistance on the particle output of a spark discharge nanoparticle generator, *J. Aerosol Sci.* 118 (2018) 59–63, <https://doi.org/10.1016/j.jaerosci.2018.01.011>.
- [40] A. Kohut, V. Horváth, Z. Pápa, B. Vajda, J. Kopiczky, G. Galbács, Z. Geretovszky, One-step fabrication of fiber optic SERS sensors via spark ablation, *Nanotechnology* 32 (2021) 395501, <https://doi.org/10.1088/1361-6528/ac0c41>.
- [41] D. Ma, P. Tiersun, L. Cheng, Y. Zheng, R. Abulaiti, PyMieLab\_V1.0: a software for calculating the light scattering and absorption of spherical particles, *Heliyon* 8 (2022) e11469, <https://doi.org/10.1016/J.HELIYON.2022.E11469>.
- [42] Scott Prah, miepython Python library, (2017).
- [43] O. Peña-Rodríguez, Modelling the dielectric function of Au–Ag alloys, *J. Alloy. Compd.* 694 (2017) 857–863, <https://doi.org/10.1016/J.JALLCOM.2016.10.086>.
- [44] P.B. Johnson, R.W. Christy, Optical constants of the Noble Metals, *Phys. Rev. B* 6 (1972) 4370, <https://doi.org/10.1103/PhysRevB.6.4370>.
- [45] K.M. McPeak, S.V. Jayanti, S.J.P. Kress, S. Meyer, S. Iotti, A. Rossinelli, D.J. Norris, Plasmonic films can easily be better: rules and recipes, *ACS Photonics* 2 (2015) 326–333, [https://doi.org/10.1021/PH5004237/SUPPL\\_FILE/PH5004237\\_SI\\_003.TXT](https://doi.org/10.1021/PH5004237/SUPPL_FILE/PH5004237_SI_003.TXT).
- [46] J.H. Weaver, S. Babar, Optical constants of Cu, Ag, and Au revisited, *Appl. Opt.* 54 (2015) 477–481, <https://doi.org/10.1364/AO.54.000477>.
- [47] A. Ciesielski, L. Skowronski, M. Trzcinski, E. Górecka, P. Trautman, T. Szoplik, Evidence of germanium segregation in gold thin films, *Surf. Sci.* 674 (2018) 73–78, <https://doi.org/10.1016/J.SUSC.2018.03.020>.
- [48] G. Rosenblatt, B. Simkhovich, G. Bartal, M. Orenstein, Nonmodal plasmonics: controlling the forced optical response of nanostructures, *Phys. Rev. X* 10 (2020) 011071, [https://doi.org/10.1103/PhysRevX.10.011071/SUPPLEMENTARY\\_MATERIAL\\_REVISED\\_PDF](https://doi.org/10.1103/PhysRevX.10.011071/SUPPLEMENTARY_MATERIAL_REVISED_PDF).
- [49] J.M. Elazar, A.B. Djurišić, A.D. Rakić, M.L. Majewski, Optical properties of metallic films for vertical-cavity optoelectronic devices, *Appl. Opt.* 37 (1998) 5271–5283, <https://doi.org/10.1364/AO.37.005271>.
- [50] Y. Hu, A.Q. Zhang, H.J. Li, D.J. Qian, M. Chen, Synthesis, study, and discrete dipole approximation simulation of Ag–Au bimetallic nanostructures, *Nanoscale Res. Lett.* 11 (2016) 1–9, <https://doi.org/10.1186/S11671-016-1435-4/FIGURES/8>.
- [51] J. Zhu, Composition-Dependent plasmon shift in Au–Ag alloy nanotubes: effect of local field distribution, *J. Phys. Chem. C* 113 (2009) 3164–3167, [https://doi.org/10.1021/JP810192F/ASSET/IMAGES/LARGE/JP-2008-10192F\\_0004.JPEG](https://doi.org/10.1021/JP810192F/ASSET/IMAGES/LARGE/JP-2008-10192F_0004.JPEG).
- [52] P. Mulvaney, Surface plasmon spectroscopy of nanosized metal particles, *Langmuir* 12 (1996) 788–800, <https://doi.org/10.1021/LA9502711/ASSET/IMAGES/LARGE/LA9502711F00017.JPEG>.
- [53] I. Russier-Antoine, G. Bachelier, V. Sablonière, J. Duboisset, E. Benichou, C. Jonin, F. Bertorelle, P.F. Brevet, Surface heterogeneity in Au–Ag nanoparticles probed by hyper-Rayleigh scattering, *Phys. Rev. B Condens. Matter Mater. Phys.* 78 (2008) 035436, <https://doi.org/10.1103/PhysRevB.78.035436/FIGURES/7/THUMBNAI>.
- [54] M. Caro, A. Caro, J. Olivares, O. Peña-Rodríguez, J.M. Perlado, A. Rivera, Optical properties of Au–Ag alloys: an ellipsometric study, *Opt. Mater. Express* 4 (2014) 403–410, <https://doi.org/10.1364/OME.4.000403>.
- [55] S.M. Morton, D.W. Silverstein, L. Jensen, Theoretical studies of plasmonics using electronic structure methods, *Chem. Rev.* 111 (2011) 3962–3994, [https://doi.org/10.1021/CR100265F/ASSET/IMAGES/MEDIUM/CR-2010-00265F\\_0032.GIF](https://doi.org/10.1021/CR100265F/ASSET/IMAGES/MEDIUM/CR-2010-00265F_0032.GIF).
- [56] H. Ma, X. Liu, C. Gao, Y. Yin, The calculated dielectric function and optical properties of bimetallic alloy nanoparticles, *J. Phys. Chem. C* 124 (2020) 2721–2727, [https://doi.org/10.1021/ACS.JPC.9B11154/ASSET/IMAGES/MEDIUM/JP9B11154\\_0001.GIF](https://doi.org/10.1021/ACS.JPC.9B11154/ASSET/IMAGES/MEDIUM/JP9B11154_0001.GIF).
- [57] K. Ripken, Die optischen Konstanten von Au, Ag und ihren Legierungen im Energiebereich 2,4 bis 4,4 eV, Z. F. üR. Phys. 250 (1972) 228–234, <https://doi.org/10.1007/BF01387459/METRICS>.
- [58] K.L. Kelly, E. Coronado, L.L. Zhao, G.C. Schatz, The optical properties of metal nanoparticles: the influence of size, shape, and dielectric environment, *J. Phys. Chem. B* 107 (2003) 668–677, <https://doi.org/10.1021/jp026731y>.
- [59] U. Kreibitz, M. Vollmer, Optical Properties of Metal Clusters, 25 (1995). <https://doi.org/10.1007/978-3-662-09109-8>.
- [60] Z.Y. Li, J.P. Wilcoxon, F. Yin, Y. Chen, R.E. Palmer, R.L. Johnston, Structures and optical properties of 4–5 nm bimetallic AgAu nanoparticles, *Faraday Discuss.* 138 (2008) 363–373, <https://doi.org/10.1039/B708958A>.
- [61] P.N. Njoki, I.I.S. Lim, D. Mott, H.Y. Park, B. Khan, S. Mishra, R. Sujakumar, J. Luo, C.J. Zhong, Size correlation of optical and spectroscopic properties for gold nanoparticles, *J. Phys. Chem. C* 111 (2007) 14664–14669, <https://doi.org/10.1021/JP074902Z/ASSET/IMAGES/LARGE/JP074902ZF000009.JPEG>.
- [62] J.P. Wilcoxon, J.E. Martin, P. Proencio, Optical properties of gold and silver nanoclusters investigated by liquid chromatography, *J. Chem. Phys.* 115 (2001) 998–1008, <https://doi.org/10.1063/1.1380374>.
- [63] A. Campos, N. Troc, E. Cottancin, M. Pellarin, H.C. Weissker, J. Lermé, M. Kociak, M. Hillenkamp, Plasmonic quantum size effects in silver nanoparticles are dominated by interfaces and local environments, *Nat. Phys.* 15 (2018) 275–280, <https://doi.org/10.1038/s41567-018-0345-z>.